Radiochim. Acta **93**, 553–560 (2005)

Experimental measurements and nuclear model calculations on the excitation functions of $^{nat}Ce(^3He, xn)$ and $^{141}Pr(p, xn)$ reactions with special reference to production of the therapeutic radionuclide ^{140}Nd

By K. Hilgers, Yu. N. Shubin†, H. H. Coenen and S. M. Qaim*

Institut für Nuklearchemie, Forschungszentrum Jülich GmbH, 52425 Jülich, Germany

(Received February 20, 2005; accepted in revised form May 9, 2005)

Neodymium-139,140,141 / Cross section / Excitation function / Nuclear model calculation / ALICE-IPPE / Therapeutic radionuclide / Integral yield

Summary. For production of the therapy related Auger electron emitting neutron deficient nuclide ^{140}Nd ($T_{1/2} = 3.37$ d) two routes were investigated: the nuclear reaction $^{nat}Ce(^3He, xn)^{140}Nd$ over the energy range from 15 to 36 MeV and the reaction $^{141}Pr(p, 2n)^{140}Nd$ from 10 to 45 MeV. Some competing reactions leading to other Nd isotopes, namely ^{139}Nd and ^{141}Nd, as well as to ^{139}Ce were also investigated. Thin samples of cerium(IV)-oxide and praseodymium(III)-oxide were obtained by sedimentation and the conventional stacked-foil technique was used for cross section measurements. All the experimental data obtained in this work were compared with the results of theoretical calculations using the exciton model code ALICE-IPPE as well as with literature experimental data, if available. In general, good agreement between experimental and theoretical results was found. The theoretical thick target yields of all the product nuclides were calculated from the measured excitation functions. The theoretical thick target yield of ^{140}Nd over the energy range $E_{^3He} = 35 \rightarrow 20$ MeV amounts to 12 MBq/μA·h and over the energy range $E_p = 30 \rightarrow 15$ MeV to 210 MBq/μA·h. A comparison of the two ^{140}Nd-producing reactions is presented.

1. Introduction

In a search for new nuclides suitable for therapeutic purposes [cf. 1, 2], the radionuclide ^{140}Nd ($T_{1/2} = 3.37$ d, 100% EC, no γ-radiation) was found to offer some unique properties suitable for therapy. The nuclide itself emits only Auger electrons [cf. 3 and the literature cited therein] and also its half-life is suitable for endoradiotherapy. Its daughter nuclide ^{140}Pr ($T_{1/2} = 3.4$ min, EC = 49.2%, $I_{\beta^+} = 50.8\%$, $E_{\beta^+} = 2.4$ MeV) brings the additional advantage of *in vivo* localisation *via* positron emission tomography (PET), thus making the radiation dosimetry more quantitative, without introducing any other β^+-emitting isotopic nuclide, as it is done, for example, in the pair $^{86}Y/^{90}Y$ [4]. Due to the low range of the Auger electrons (mean energy 6 keV [3]), the therapy effect is very specific, provided the nuclide can be brought to the cell nucleus.

For the production of ^{140}Nd different routes are possible:

a) $^{141}Pr(p, 2n)^{140}Nd$ and $^{141}Pr(d, 3n)^{140}Nd$ reactions,
b) $^{nat}Ce(^3He, xn)^{140}Nd$ and $^{nat}Ce(\alpha, xn)^{140}Nd$ processes,
c) spallation of materials like tantalum.

In this work we concentrated on the $^{nat}Ce(^3He, xn)^{140}Nd$ and $^{141}Pr(p, 2n)^{140}Nd$ reactions. The production of ^{140}Nd *via* the $^{nat}Ce(^3He, xn)^{140}Nd$ reaction as well as a preliminary application have been demonstrated earlier [3]. Any detailed data measurements, however, have hitherto not been reported. For the reaction $^{141}Pr(p, 2n)^{140}Nd$ two data sets were available in the literature [5, 6], but with conflicting results. In the present work we studied those two processes in detail and also measured cross sections for some competing reactions. For comparison, nuclear model calculations were carried out using the code ALICE-IPPE for all the reactions under investigation.

2. Experimental

The conventional stacked-foil technique was used for cross section measurements. Some of the salient features relevant to the present work are given below.

2.1 Sample preparation

CeO_2 and Pr_2O_3 of natural isotopic composition and high chemical purity (99.999%, Koch-Light Laboratories, UK) were used to prepare thin samples by sedimentation. About 10 mg of the respective oxide together with 4%–5% of nitrocellulose were suspended in acetone (99.7%). This suspension was introduced in a sedimentation cell consisting of a teflon disc as bottom and a teflon ring on top. In between those teflon parts a 25 μm thick Cu foil (99.9% pure, Goodfellow, UK) with a diameter of 13 mm served as the backing of the sample [cf. 7, 8]. After evaporation of the acetone the sample was taken out, the uniformity of the deposit checked using a microscope and the sample was covered and

*Author for correspondence (E-mail: s.m.qaim@fz-juelich.de).
† Guest scientist from Institute of Physics and Power Engineering, Obninsk, Russia. Now deceased.

wrapped up at the margin by a thin Al foil (thickness 10 μm, diameter 16 mm, 99.9% pure, Goodfellow, UK).

2.2 Irradiations and beam monitoring

Irradiations were carried out using the conventional stacked-foil technique [cf. 9, 10]. Protons of energies 12, 16 and 20 MeV and ^{3}He-particles of energies 25 and 36 MeV were extracted from the compact cyclotron CV 28 and protons of energy 45 MeV from the injector of COSY, both accelerators available at Forschungszentrum Jülich GmbH. Several stacks consisting of the thin samples of the respective oxide and thin Ti and Cu monitor foils (both > 99.6%, Goodfellow, UK) were irradiated. The charged particle flux on the target was measured by charge integration as well as *via* the monitor reactions ^{nat}Ti(^{3}He, x)^{48}V, ^{nat}Ti(p, x)^{48}V and ^{nat}Cu(p, x)^{62,65}Zn. The cross sections of those monitor reactions were taken from an evaluated data file [11]. The calculation of energy degradation within each stack was based on the method of Williamson *et al.* [12].

2.3 Measurement of radioactivity

For activity measurement, in each case a HPGe detector was used and the γ-ray spectrum recorded several times to check the half-life of the product. In the case of ^{140}Nd, the activity was measured using the annihilation peak of the daughter nuclide ^{140}Pr ($T_{1/2} = 3.4$ min). The measurement of this nuclide was started at least three days after end of bombardment (EOB). By this time most of the short-lived products had decayed out and a complete equilibrium between ^{140}Nd and ^{140}Pr was assured. This fact and the ratio of the half-lives of these two nuclides (secular equilibrium) allowed a neglect of the decay of ^{140}Pr. Also in the case of ^{141}Nd the activity was partially measured using the annihilation radiation. It should be mentioned that while measuring the activity using the annihilation peak, the samples were covered with two 2 mm thick copper plates to assure the complete annihilation of the positrons in a small volume around the samples. The efficiency of the detector was measured in the same geometry. A careful decay curve analysis was undertaken by a series of measurements over at least three half-lives of the respective nuclide. All the other nuclides were identified by their respective γ-rays, which are listed in Table 1. In those cases also the half-lives were checked. In general, the samples were measured at a distance of 10 cm from the detector while looking for the longer-lived products, and at distances between 10 and 50 cm from the detector in case of shorter-lived products. The monitor foils were measured at distances between 10 and 50 cm. The detectors were calibrated with standard sources supplied by the Physikalisch-Technische Bundesanstalt (PTB) and Amersham International. The decay data of all the investigated radionuclides were taken from the Tables of Isotopes [13]. The activity of each product was obtained by averaging the results of various measurements extrapolated to EOB. The absolute activity was then derived by applying the usual corrections like those for γ-ray intensity, detector efficiency, *etc.*

Table 1. Investigated nuclides and their decay properties[a].

Investigated nuclide	Half-life	γ-rays used for activity measurement [keV]	Intensity [%]
^{141}Nd	2.5 h	511	2.5
		1127	0.8
^{140}Nd	3.37 d	511 (from daughter ^{140}Pr)	101.6
^{139g}Nd	29.7 min	405	6.9
^{139m}Nd	5.5 h	708	26
		739	35
^{139g}Ce	137.6 d	166	79.9

a: taken from [13].

2.4 Calculation of cross section and uncertainty

To calculate the beam flux from the beam monitor activity, the activation equation was used with the known monitor cross section as mentioned above. With this beam flux and the reaction product activity, the cross section was calculated, again using the activation equation. For estimation of uncertainties see Table 2. The uncertainty in the primary proton energy amounted to 0.2 MeV. For ^{3}He-induced reactions the uncertainty was 0.5 MeV in the first foils because of the higher energy degradation of ^{3}He in the matter. The uncertainty in the energy effective at each foil increased with the increasing number of foils.

3. Nuclear model calculations

For an interpretation and validation of our data, nuclear model calculations using the ALICE-IPPE code were performed. This code is a modified version of ALICE, which is based on the exciton model [14]. In the code used in this work, the following modifications have been introduced [15]:

– treatment of level density in a generalized superfluid model,

Table 2. Uncertainties and their magnitudes in cross section measurements.

Source of uncertainty	Estimated magnitude
Uncertainty in number of target nuclei	2–5%
Uncertainty in target uniformity	3–5%
Uncertainty in efficiency of the detector	4–6%
Uncertainty in peak area	2–8%
Uncertainty in cross section of monitor reaction	8–10%
Uncertainty in decay data	1%
Total uncertainty in measured cross section	10–20%
Uncertainty in projectile energy effective at a sample	0.2 to 1 MeV

– consideration of preequilibrium cluster emission,
– estimation of direct interactions in cluster emission.

This code has been very successful in describing (p, xn) reactions [cf. 16, 17] and (p, pxn) processes [cf. 18] in medium mass regions, even when standard input parameters were used. In this work the ALICE-IPPE code was applied to calculate both (p, xn) and (^{3}He, xn) reactions. In the case of cerium it was necessary to consider its isotopic composition (0.16% ^{136}Ce, 0.25% ^{138}Ce, 88.48% ^{140}Ce and 11.08% ^{142}Ce). Only the major isotopes ^{140}Ce and ^{142}Ce were taken into account in the calculations. As far as we know, calculations on ^{3}He-induced reactions have been done for the first time using ALICE-IPPE.

4. Results and discussion

4.1 Cross sections

The measured cross sections for the ^{nat}Ce(^{3}He, xn) reactions and the ^{nat}Ce(^{3}He, x)^{139}Ce process are given in Table 3 and those for the ^{141}Pr(p, xn) reactions and the ^{141}Pr(p, x)^{139}Ce process in Table 4. Below each investigated reaction is discussed individually.

4.1.1 Cross sections for ^{3}He-particle induced reactions

No data existed in the literature for these reactions. Our measured data are therefore only compared with the results of the ALICE-IPPE calculations.

^{nat}Ce(^{3}He, xn)^{141}Nd process

As can be seen in Table 1, ^{141}Nd emits only γ-rays of weak intensities. The annihilation radiation could not be used for measuring the activity of this nuclide, because this radiation is not specific. Especially the nuclide ^{18}F (produced *via* the ^{16}O(^{3}He, p) reaction) with its similar half-life and high intensity annihilation radiation made it impossible to use this radiation for determining the activity of ^{141}Nd. Therefore the γ-ray at 1127 keV was used for calculation. Since the intensity is very weak (0.8%), the uncertainty in the peak area is higher for this reaction, which is taken into account in the values given in Table 2. The experimental values for this reaction are shown in Fig. 1 together with the ALICE-IPPE calculations. The experimental results show a threshold at about 12 MeV and two maxima at about 19 and 32 MeV, which are attributed to ^{140}Ce(^{3}He, 2n) and ^{142}Ce(^{3}He, 4n) processes, re-

Table 3. Measured cross sections of the ^{nat}Ce(^{3}He, xn)^{141,140,139}Nd and ^{nat}Ce(^{3}He, x)^{139}Ce reactions.

Projectile energy	Cross section [mb]			
[MeV]	^{nat}Ce(^{3}He, xn)^{141}Nd	^{nat}Ce(^{3}He, xn)^{140}Nd	^{nat}Ce(^{3}He, xn)^{139}Nd	^{nat}Ce(^{3}He, x)^{139}Ce
35.2 ± 0.5	142 ± 28		539 ± 162	
35.0 ± 0.5		442 ± 75		377 ± 57
34.2 ± 0.5	131 ± 26			
34.0 ± 0.5		545 ± 93		330 ± 50
33.8 ± 0.5	126 ± 25		344 ± 103	
33.2 ± 0.5			252 ± 76	
32.9 ± 0.5		606 ± 103		227 ± 34
32.8 ± 0.5	192 ± 38			
32.0 ± 0.5	230 ± 46		313 ± 94	
31.7 ± 0.6		592 ± 101		167 ± 25
30.4 ± 0.6		624 ± 106	76 ± 23	78 ± 12
29.7 ± 0.6	138 ± 28			
29.1 ± 0.7			76 ± 23	
28.2 ± 0.7		665 ± 113		36 ± 2
27.7 ± 0.7			9 ± 3	
27.0 ± 0.7		613 ± 104		17 ± 3
26.6 ± 0.6	181 ± 36			
26.1 ± 0.7		818 ± 139		15 ± 2
24.1 ± 0.5		641 ± 109		
23.4 ± 0.5		410 ± 70		7 ± 1
23.0 ± 0.7	173 ± 35			
22.0 ± 0.5		234 ± 40		5 ± 1
21.5 ± 0.7	180 ± 36			
20.8 ± 0.6		196 ± 33		6 ± 1
19.8 ± 0.8	247 ± 49			
18.6 ± 0.8	173 ± 35			
18.3 ± 0.7		104 ± 18		3 ± 0.5
17.7 ± 0.8		139 ± 24		6 ± 1
17.6 ± 0.8		80 ± 14		3 ± 0.5
17.4 ± 0.8	38 ± 8			
16.9 ± 0.8		91 ± 15		
16.5 ± 0.9	60 ± 12			5 ± 1
16.3 ± 0.9	104 ± 21			
16.0 ± 0.8		23 ± 4		
15.9 ± 0.9		11 ± 2		
15.0 ± 0.9	59 ± 12			

Table 4. Measured cross sections of the ^{141}Pr$(p, xn)^{141,140,139}$Nd and ^{141}Pr$(p, x)^{139}$Ce reactions.

Projectile energy	Cross section [mb]			
[MeV]	^{141}Pr$(p, n)^{141}$Nd	^{141}Pr$(p, 2n)^{140}$Nd	^{141}Pr$(p, 3n)^{139}$Nd	^{141}Pr$(p, x)^{139}$Nd
44.8 ± 0.2		135 ± 20	116 ± 35	521 ± 78
43.8 ± 0.2		67 ± 10	208 ± 62	394 ± 59
42.1 ± 0.3		132 ± 20		
41.6 ± 0.3		184 ± 28	438 ± 131	632 ± 95
41.6 ± 0.3				542 ± 81
40.0 ± 0.3		154 ± 23		
39.1 ± 0.4		125 ± 19	474 ± 142	653 ± 98
39.0 ± 0.4		105 ± 16		595 ± 89
37.6 ± 0.5		88 ± 13		776 ± 116
36.7 ± 0.5		160 ± 24		989 ± 148
35.0 ± 0.5		132 ± 20		906 ± 136
34.9 ± 0.5		168 ± 25		901 ± 135
34.3 ± 0.5		159 ± 24		1067 ± 160
32.9 ± 0.6		212 ± 32	789 ± 237	
30.9 ± 0.6		226 ± 34		1021 ± 153
30.4 ± 0.6		261 ± 39	1017 ± 305	1103 ± 165
29.8 ± 0.6		358 ± 54		
29.5 ± 0.7		122 ± 18	720 ± 216	
29.3 ± 0.7		273 ± 41		
27.0 ± 0.7		521 ± 125		745 ± 112
26.6 ± 0.7		1029 ± 154	567 ± 170	922 ± 138
25.3 ± 0.8		1182 ± 177	379 ± 114	429 ± 64
23.8 ± 0.9			17 ± 5	88 ± 13
23.3 ± 0.9		1292 ± 194		
21.0 ± 1.0		1174 ± 176	1.2 ± 0.4	
21.0 ± 1.0		1366 ± 205		
20.0 ± 1.0		910 ± 137		
19.3 ± 0.2		833 ± 125		
18.1 ± 0.3		923 ± 139		
18.0 ± 1.0		722 ± 108		
17.1 ± 0.3	87 ± 13			
16.9 ± 0.4		826 ± 124		
15.5 ± 0.5		590 ± 89		
15.1 ± 0.2		283 ± 43		
14.3 ± 0.3	346 ± 52	494 ± 74		
13.9 ± 0.6		417 ± 63		
13.6 ± 0.3	325 ± 49			
12.9 ± 0.4	351 ± 53			
12.5 ± 0.4		19 ± 3		
12.3 ± 0.4	599 ± 90			
11.5 ± 0.5	577 ± 87			
11.4 ± 0.5	409 ± 61			
10.6 ± 0.6		21 ± 3		
10.4 ± 0.7	295 ± 44			
10.2 ± 0.6	418 ± 63			
10.0 ± 0.4	347 ± 52			
9.8 ± 0.7	264 ± 40			
8.0 ± 0.5	51 ± 8			

spectively. The theoretical curve follows approximately the same shape.

^{nat}Ce$(^3$He, $xn)^{140}$Nd *process*

The results for this reaction are shown in Fig. 2. The experimentally found threshold lies at about 16 MeV and the maximum cross section of around 800 mb occurs at 27 MeV. The formation of ^{140}Nd up to 27 MeV entails predominantly the ^{140}Ce$(^3$He, $3n)^{140}$Nd process. Going to higher energies, the ^{142}Ce$(^3$He, $5n)^{140}$Nd reaction can also contribute to the production of ^{140}Nd. For this reaction, the experimental data and the results of ALICE-IPPE calculations (also shown in Fig. 2) agree fairly well, except in the threshold region and at energies above 26 MeV. The calculated threshold is somewhat shifted to higher energy and in the higher energy region the theoretical values are 20%–30% higher than the experimental data.

^{nat}Ce$(^3$He, $xn)^{139}$Nd *process*

To determine the total cross section for all channels leading to ^{139}Nd, both the isomeric and the ground states had to be measured and the cross sections were added. The uncertainty for this cross section is therefore higher than for the other reactions. Furthermore, the ground state had to be corrected for the internal transition (11.8%) of the isomeric state to the ground state. The data for this reaction are given

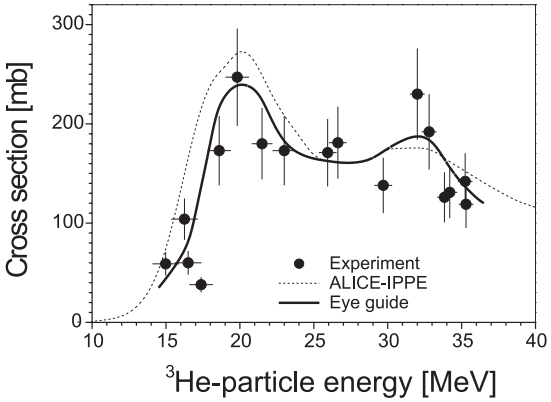

Fig. 1. Experimental cross-section data for the ^{nat}Ce(^{3}He, xn)^{141}Nd reaction and results of ALICE-IPPE calculations. The eye-guide curve follows the experimental results. The first peak in the excitation function is attributed to the ^{140}Ce(^{3}He, $2n$)^{141}Nd reaction and the second one to the ^{142}Ce(^{3}He, $4n$)^{141}Nd reaction.

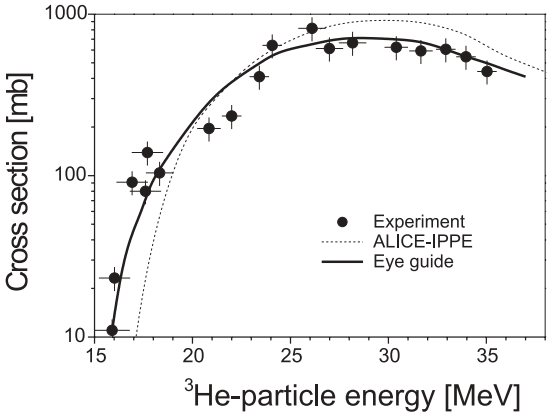

Fig. 2. Experimental cross-section data for the ^{nat}Ce(^{3}He, xn)^{140}Nd reaction and results of ALICE-IPPE calculations. The eye-guide curve follows the experimental results. The main contributing process is the ^{140}Ce(^{3}He, $3n$)^{140}Nd reaction.

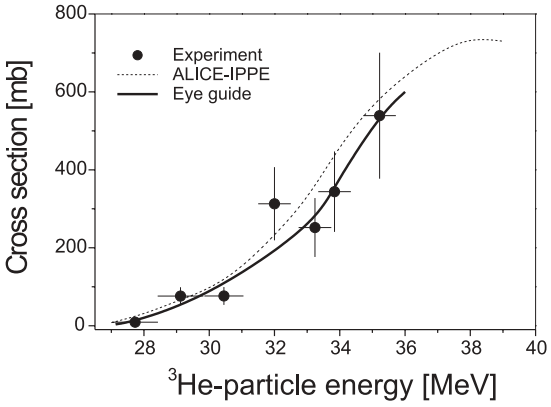

Fig. 3. Experimental cross-section data for the ^{nat}Ce(^{3}He, xn)^{139}Nd reaction and results of ALICE-IPPE calculations. The eye-guide curve follows the experimental results. The main contributing process is the ^{140}Ce(^{3}He, $4n$)^{139}Nd reaction.

in Fig. 3. A reaction threshold of about 27 MeV is observed but no maximum in the cross section is reached till 36 MeV. It is almost a pure ^{140}Ce(^{3}He, $4n$)^{139}Nd reaction. The experimental results are in good agreement with the ALICE-IPPE calculations, also shown in Fig. 3 for comparison.

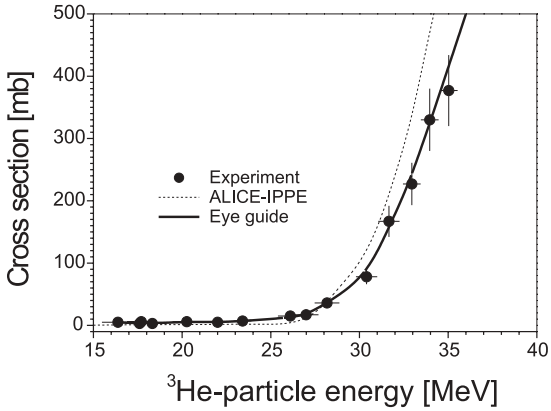

Fig. 4. Experimental cross-section data for the ^{nat}Ce(^{3}He, x)^{139}Ce reaction and results of ALICE-IPPE calculations. The eye-guide curve follows the experimental results. The cross section describes the sum of ^{140}Ce(^{3}He, $4n$)^{139}Nd → ^{139}Pr → ^{139}Ce and ^{140}Ce(^{3}He, α)^{139}Ce processes.

^{nat}Ce(^{3}He, x)^{139}Ce *process*

The ^{139}Ce formation cross section given here is the cumulative cross section of the processes ^{nat}Ce(^{3}He, x)^{139}Nd, ^{nat}Ce(^{3}He, x)^{139}Pr and ^{nat}Ce(^{3}He, x)^{139}Ce, the first two decaying to ^{139}Ce. The ALICE-IPPE calculations for this reaction channel are also based on these three reactions. The results are shown in Fig. 4. The reaction has a threshold of about 16 MeV but no maximum in the cross section is reached till 36 MeV. The theoretical calculations for this process, also given in Fig. 4, are in good agreement with the experimental results up to 28 MeV. Going to higher energies the calculations show a significantly higher cross section compared to the experimental data.

In summary, considering that ^{3}He is a loosely bound projectile, the agreement between theoretical and experimental results for all the investigated nuclear processes may be regarded as satisfactory.

4.1.2 Cross sections for proton induced reactions

^{141}Pr(p, n)^{141}Nd *reaction*

In this case both the annihilation radiation and the γ-ray at 1127 keV could be used for calculating the activity of ^{141}Nd. Both methods gave consistent results. In this case the disturbance from ^{18}F, formed *via* the ^{18}O(p, n)-reaction, was negligible due to the very low abundance of ^{18}O (0.2%) in ^{nat}O. Our experimental results and the literature data for this reaction are given in Fig. 5. The reaction threshold lies at about 5 MeV and a maximum cross section of around 600 mb at approximately 12 MeV is observed. The results of ALICE-IPPE calculations are also given in Fig. 5. Our data agree with the experimental data of Olkowsky *et al.* [19] in the low energy region and with those of Grytsina *et al.* [20] in the higher energy region. The data by Hogan [5] are too scanty to show a trend. The calculated results are in agreement with our experimental data around the maximum of the excitation function. The theoretical results are also in agreement with the data of Hogan [5] and Grytsina *et al.* [20] in the increasing part of the excitation function, but not with the other values [19, this work]. On the other hand, compared to all sets of experimental data (except the data of Hogan [5]), the

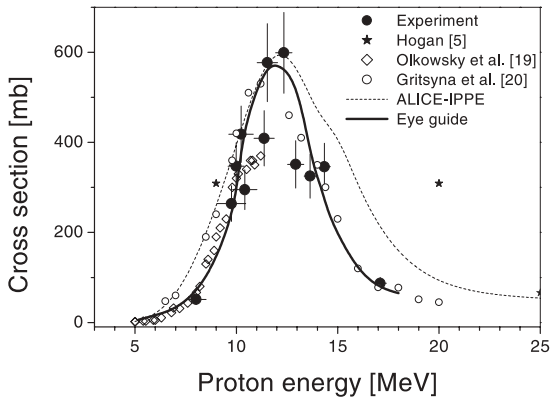

Fig. 5. Experimental cross-section data for the ^{141}Pr$(p, n)^{141}$Nd reaction and results of ALICE-IPPE calculations. The eye-guide curve follows the experimental results.

theoretical results give a much broader flank on the decreasing side of the excitation function. Apparently the exciton model is not very successful in describing the (p, n) process, especially after the maximum of the excitation curve.

^{141}Pr$(p, 2n)^{140}$Nd *reaction*

The experimental data obtained in this work and those reported in the literature together with the results of theoretical calculations are given in Fig. 6. The reaction has a threshold of about 10 MeV and a maximum cross section of 1300 mb at about 20 MeV. Whereas the values by Hogan [5] show a higher cross section, the data of this work and those by Zeisler and Becker [6] are in excellent agreement except near the threshold. As far as the results of the ALICE-IPPE calculations are concerned, there is some deviation from the experimental data in the threshold region but an excellent agreement at energies above 20 MeV. It should be pointed out that we obtained the full excitation function of this reaction using two cyclotrons (CV 28 and injector of COSY). The consistency in data in the overlapping region adds confidence to the obtained results. A second point worth mentioning is that Zeisler and Becker [6] used a completely different technique. The good agreement between their and our data shows that the yield of ^{140}Nd can reliably be calculated using the now available database.

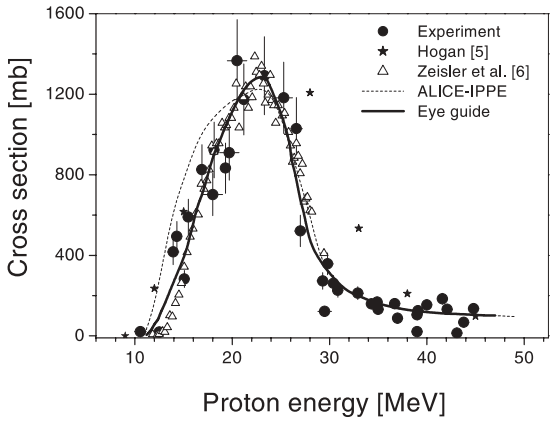

Fig. 6. Experimental cross-section data for the ^{141}Pr$(p, 2n)^{140}$Nd reaction and results of ALICE-IPPE calculations. The eye-guide curve follows the experimental results.

^{141}Pr$(p, 3n)^{139}$Nd *reaction*

The experimental data from this work and those reported in the literature as well as the results of nuclear model calculations are given in Fig. 7. Similar to ^{3}He-induced reactions, the cross section for this process is the sum of the cross sections for the formation of the two states of this nuclide. The threshold of the reaction is at about 22 MeV and the maximum cross section around 32 MeV amounts to about 1000 mb. Except for one scattered point of Hogan [5], these data and the experimental results of Vermeulen *et al.* [21] appear to be in good agreement with our data as well as with the theoretical calculations.

^{141}Pr$(p, x)^{139}$Ce *process*

The ^{139}Ce formation cross section given here, similar to the description of the $^{\text{nat}}$Ce$(^{3}\text{He}, x)^{139}$Ce process, is the cumulative cross section of the processes ^{141}Pr$(p, 3n)^{139}$Nd, ^{141}Pr$(p, x)^{139}$Pr and ^{141}Pr$(p, x)^{139}$Ce. The ALICE-IPPE calculations for this reaction channel are also based on those three reactions. The results are shown together with the literature data in Fig. 8. This nuclear process has a threshold of about 22 MeV and a maximum cross section of 1200 mb at 32 MeV. The ALICE-IPPE calculations and all experimental results are in agreement, although around the maximum the

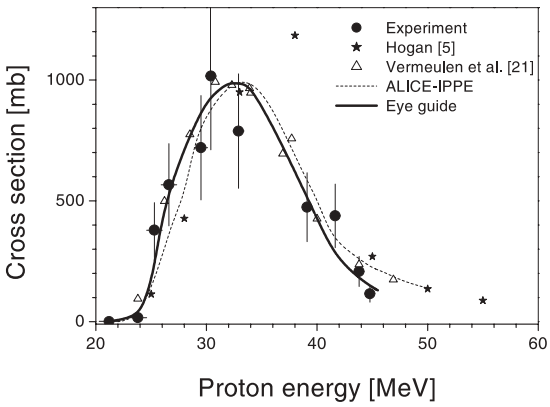

Fig. 7. Experimental cross-section data for the ^{141}Pr$(p, 3n)^{139}$Nd reaction and results of ALICE-IPPE calculations. The eye-guide curve follows the experimental results.

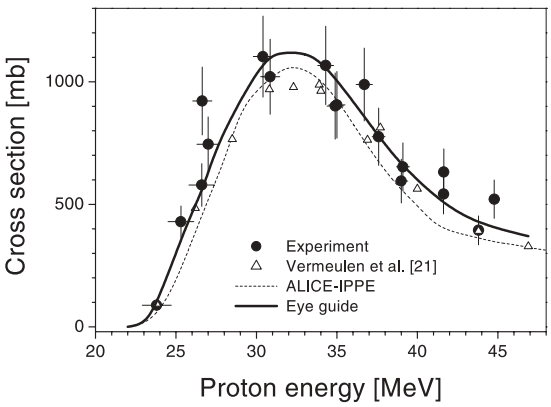

Fig. 8. Experimental cross-section data for the ^{141}Pr$(p, x)^{139}$Ce reaction and results of ALICE-IPPE calculations. The eye-guide curve follows the experimental results. The cross section describes the sum of ^{141}Pr$(p, 3n)^{139}$Nd $\rightarrow$ ^{139}Pr $\rightarrow$ ^{139}Ce and ^{141}Pr$(p, 2pn)^{139}$Ce processes.

data of Vermeulen *et al.* [21] show somewhat better agreement with the theoretical calculation.

4.2 Thick target yields

The integrated yield of each investigated radionuclide *via* a nuclear reaction was calculated from the eye-guide curve given in the respective figure. Each eye guide depicts a smooth line through our experimental results. It follows approximately the Table curve fitting. For the yield calculation, the activation equation was used, with the particle flux corresponding to 1 μA (6.24×10^{12} particles/s in case of protons, 3.12×10^{12} particles/s in case of ^{3}He). The irradiation time was assumed as 1 h. The results are given in Fig. 9 for ^{3}He-particle induced reactions on ^{nat}Ce and in Fig. 10 for proton induced reactions on ^{141}Pr, both as a function of projectile energy.

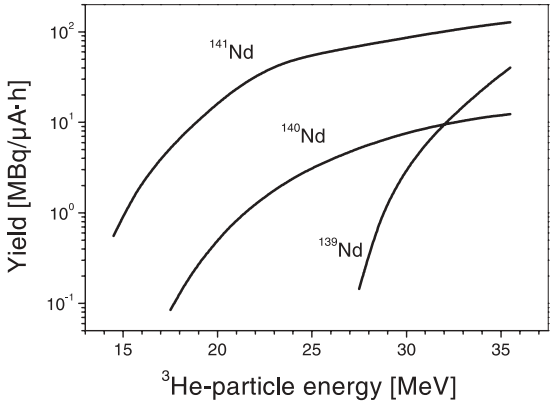

Fig. 9. Integral yields of ^{141,140,139}Nd calculated from the excitation functions of the ^{3}He-particle induced reactions on ^{nat}Ce (eye-guide curves given in Figs. 1–3) shown as a function of incident particle energy.

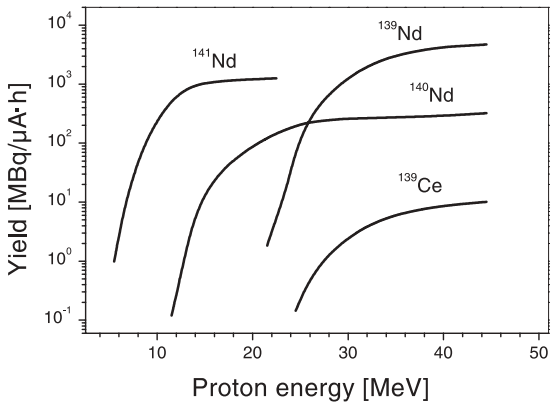

Fig. 10. Integral yields of ^{141,140,139}Nd and ^{139}Ce calculated from the excitation functions of proton induced reactions on ^{141}Pr (eye-guide curves given in Figs. 5–8) shown as a function of proton energy.

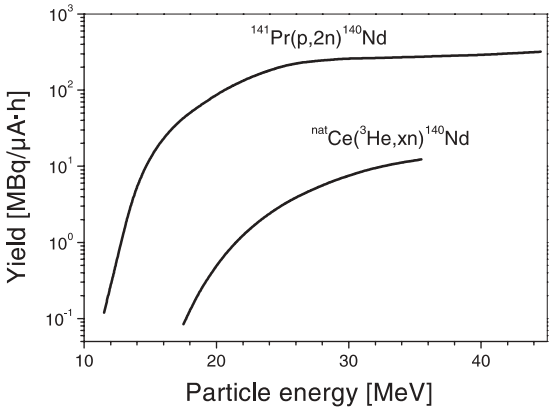

Fig. 11. Comparison of the integral yield of ^{140}Nd in the proton and ^{3}He-particle induced reactions as a function of the incident particle energy.

4.3 Comparison of production routes of ^{140}Nd

For a comparison of the two reactions for the production of ^{140}Nd, *viz.* $^{nat}Ce(^3He, xn)^{140}Nd$ and $^{141}Pr(p, 2n)^{140}Nd$, the relevant data are given in Table 5 and a direct comparison of the yields *via* both reactions is given in Fig. 11. Some important considerations are briefly discussed below. The isotopic impurities in both routes are negligible, since by the time radioneodymium is chemically separated (usually more than one day), even the longest lived impurity ^{139m}Nd has almost fully decayed. Considering the yield, the $^{141}Pr(p, 2n)^{140}Nd$ reaction is superior, its yield being about 20 times higher than the yield of the $^{nat}Ce(^3He, xn)^{140}Nd$ reaction. In terms of chemical separation of ^{140}Nd from the bulk target material, for both reactions considerable effort is needed [3, 6]. The quality in terms of chemical purity is good in both cases, but the specific activity depends on the neodymium impurity present in the respective target material. Due to the high chemical similarity of praseodymium and neodymium it seems easier to get highly pure cerium than praseodymium as target material. This could be an advantage in case of the $^{nat}Ce(^3He, xn)^{140}Nd$ reaction. However, taking all the points into account, the $^{141}Pr(p, 2n)^{140}Nd$ reaction appears to be more suitable for the production of ^{140}Nd.

5. Conclusions

A comparison of the experimental data and results of exciton-precompound model calculations using the code ALICE-IPPE showed that, in general, the theory reproduces the data fairly well. Only in some cases significant deviations occurred. For the ^{3}He-particle induced reactions, such calculations have been done for the first time. As far as practical applications of the data are concerned, the information reported in this work should provide

Table 5. Comparison of ^{140}Nd-producing reactions.

Production route	E_{max} [MeV]	σ_{max} [mb]	Suitable energy range [MeV]	Integral yield [MBq/μA·h]
$^{nat}Ce(^3He, xn)^{140}Nd$	27	800	35 → 20	12
$^{141}Pr(p, 2n)^{140}Nd$	20	1300	30 → 15	210

a strong database for the production of the therapeutic radionuclide ^{140}Nd.

Acknowledgment. We thank the operators of the compact cyclotron CV 28 and the injector of COSY at the Forschungszentrum Jülich GmbH for performing the irradiations, and Mr. S. Spellerberg for technical assistance. This work was partly done under the COST action "Therapeutic Lanthanides" (D18) of the EU (Brussels).

References

1. Stöcklin, G., Qaim, S. M., Rösch, F.: The impact of radioactivity on medicine. Radiochim. Acta **70**/**71**, 249 (1995).
2. Qaim, S. M.: Therapeutic radionuclides and nuclear data. Radiochim. Acta **89**, 297 (2001).
3. Rösch, F., Brockmann, J., Lebedev, N. A., Qaim, S. M.: Production and radiochemical separation of the Auger electron emitter ^{140}Nd. Acta Oncol. **39**, 727 (2000).
4. Herzog. H., Rösch, F. Stöcklin, G. Lueders, C., Qaim, S. M., Feinendegen, L. E.: Measurement of pharmacokinetics of yttrium-86 radiopharmaceuticals with PET and radiation dose calculation of analogous yttrium-90 radiotherapeutics. J. Nucl. Med. **34**, 2222 (1993).
5. Hogan, J. J.: Study of the ^{141}Pr(p, xn) reactions from 10–85 MeV. J. Inorg. Nucl. Chem. **33**, 3627 (1971).
6. Zeisler, S., Becker, D.: Production of the ^{140}Nd/^{140}Pr radionuclide generator for biomedical studies. J. Label. Compd. Radiopharm. **42** (Suppl. 1), 921 (1999).
7. Rösch, F., Qaim, S. M., Stöcklin, G.: Nuclear data relevant to the production of the positron emitting radioisotope ^{86}Y *via* the ^{86}Sr (p, n)- and ^{nat}Rb(^{3}He, xn)-processes. Radiochim. Acta **61**, 1 (1993).
8. Denzler, F.-O., Rösch, F., Qaim, S. M.: Excitation functions of α-particle induced nuclear reactions on highly enriched ^{92}Mo: comparative evaluation of production routes for ^{94m}Tc. Radiochim. Acta **68**, 13 (1995).
9. Qaim, S. M., Stöcklin, G., Weinreich, R.: Excitation functions for the formation of neutron deficient isotopes of bromine and krypton *via* high-energy deuteron induced reactions on bromine – production of ^{77}Br, ^{76}Br and ^{79}Kr. Int. J. Appl. Radiat. Isotopes **28**, 947 (1977).
10. Mushtaq, A., Qaim, S. M.: Excitation functions of α- and ^{3}He-particle induced nuclear reactions on natural germanium: evaluation of production routes for ^{73}Se. Radiochim. Acta **50**, 27 (1990).
11. Tárkányi, T. F., Gul, K., Hermanne, A., Mustafa, M. G., Nortier, F. M., Qaim, S. M., Scholten, B., Shubin, Yu., Takács, S., Zhuang, Y.: "Beam monitor reactions". In: Charged-Particle Cross Section Database for Medical Radioisotope Production. IAEA-TECDOC-1211 (2001) p. 49.
12. Williamson, C. F., Boujot, J. P., Picard, J.: Tables of range and stopping power of chemical elements for charged particles of energies from 0.5 to 500 MeV. Rapport CEA-R 3042 (1966).
13. Firestone, R. B.: *Tables of Isotopes*. CDROM-Edn., Version 1.0, Wiley-Interscience, New York (1996).
14. Blann, M.: Preequilibrium decay. Ann. Rev. Nucl. Sci. **25**, 123 (1975).
15. Dityuk, A. I., Konobeyev, A. Yu., Lunev, V. P., Shubin, Yu. N.: New advanced version of computer code ALICE-IPPE. International Atomic Energy Agency, Vienna, Austria INDC(CCP)-410 (1998).
16. Fassbender, M., Shubin, Yu. N., Lunev, V. P., Qaim, S. M.: Experimental studies and nuclear model calcuculations on the formation of radioactive products in interactions of medium energy protons with copper, zinc and brass: estimation of collimator activation in proton therapy facilities. Appl. Radiat. Isotopes **48**, 1 (1997).
17. Hohn, A., Nortier, F. M., Scholten, B., van der Walt, T. N., Coenen, H. H., Qaim, S. M.: Excitation functions of ^{125}Te(p, xn)-reactions from their respective thresholds up to 100 MeV with special reference to the production of ^{124}I. Appl. Radiat. Isotopes **55**, 149 (2001).
18. Kastleiner, S., Shubin, Yu. N., Noriter, F. M., van der Walt, T. N., Qaim, S. M.: Experimental studies and nuclear model calculations on (p, xn) and (p, pxn) reactions on ^{85}Rb from their respective thresholds up to 100 MeV. Radiochim. Acta **92**, 449 (2004).
19. Olkowsky, J., Le Pape, M., Gratot, I.: Fonction d'excitation de ^{141}Pr(p, n)^{141}Nd jusqu'à 11.1 MeV. Nucl. Phys. **23**, 164 (1961).
20. Gritsyna, V. T., Klyucharev, A. P., Remaev, V. V., Reshetova, L. N.: Ratio of the cross sections for the production of the isomer and ground states of nuclei in the (p, n) reaction at energies from the threshold to 20 MeV. Soviet Phys. JETP **17**(6), 1186 (1963).
21. Vermeulen, C., Steyn, G. F., Nortier, F. M., van der Walt, T. N., Szelecsényi, F., Kovács, Z., Qaim, S. M.: Excitation functions and production rates of radionuclides produced in the proton bombardment of ^{nat}Pr and ^{nat}La. Int. Conf. Nuclear Data for Science and Technology, Santa Fe, USA, September (2004), AIP Conference Proceedings, Vol. 769 (Haight, R. C., Chadwick, W. B., Kawano, T., Talou, P., eds.), Melville, New York (2005), p. 1650.